2017 IEEE/RSJ International Conference on Intelligent Robots and Systems (IROS)
September 24–28, 2017, Vancouver, BC, Canada

A Novel Building Post-Construction Quality Assessment Robot: Design and Prototyping

Rui-Jun Yan[1], Erdal Kayacan[1], *Senior Member, IEEE* I-Ming Chen[1], *Fellow, IEEE* and Lee Kong Tiong[2]

***Abstract*— This paper describes the design and development of an automated construction quality assessment robot system (QuicaBot) for hollowness, crack, evenness, alignments and inclination problems. To the best of our knowledge, this work is the first attempt to pave the way towards a fully autonomous robotic system for post construction quality assessment of buildings. The main goal of the novel robot is twofold: to systematize the manual inspection work through automation resulting in more reliable and objective inspection reports, and to speed up the inspection process resulting in a cost reduction. Based-on our initial on-site tests, the developed robot increases the overall efficiency in all the aforementioned five problems.**

I. INTRODUCTION

Post construction quality assessment of buildings is an indispensable procedure in construction industry which is currently executed by manual inspectors. In a standard daily operation, 2-3 inspectors are needed to complete the manual assessment procedure. Such a fully manual inspection is subjected to several errors because of executing the operation in an incorrect way or the use of inaccurate inspection tools. What is more, the inspection accuracy may decrease over time. Last but not the least, in most of the time, manual inspection has to be done during the daytime. Motivated by this time-consuming, tiresome and unexciting procedure, we propose a novel automated post construction quality assessment robot system as shown in Fig. 1. The proposed system consists of a cloud-based mobile robot, a 2D laser scanner, a color camera, a thermal camera, a heater and an inclinometer, which have been technically validated for their assessment capabilities [1]. Even though aerial vehicles are usually used to inspect a dam [2] or vessel [3], a mobile vehicle is selected in this research considering the loading capacity and inspection stability. To the best of our knowledge, this work is the first attempt to pave the way towards a fully autonomous robotic system for post construction quality assessment of buildings.

Even if there are more problems in construction quality assessment operations which are still manually inspected, only five of them are considered in this investigation: hollowness, crack, evenness, alignment, and inclination. Motivated by the developments in infrared thermography technology

[1]Rui-Jun Yan, Erdal Kayacan, and I-Ming Chen are with the Robotics Research Center, School of Mechanical and Aerospace Engineering, Nanyang Technological University, Singapore, 639798 hityrj@outlook.com; erdal@ntu.edu.sg; michen@ntu.edu.sg

[2]Lee Kong Tiong is with the School of Civil and Environmental Engineering, Nanyang Technological University, Singapore, 639798 clktiong@ntu.edu.sg

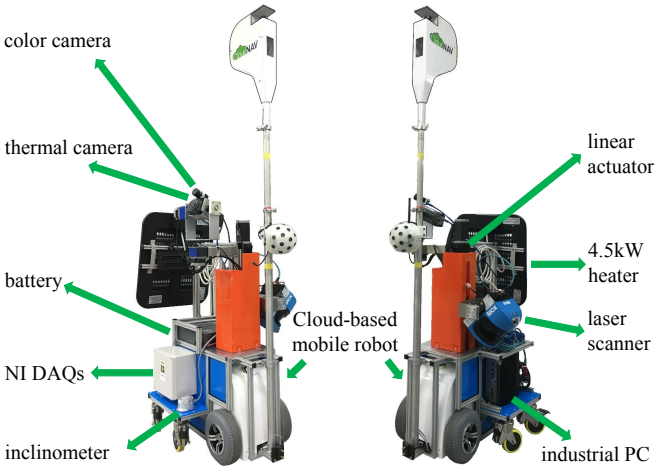

Fig. 1: A novel post-construction quality assessment robot.

[4], [5], a thermal camera is preferred for hollowness assessment. For automatic crack assessment, many researches have proposed the use of color cameras for some specific environments, such as subway tunnel [6], flexible pavement surfaces [7], [8], and bridge decks [9]. Motivated by these successful applications, a color camera is preferred for the crack detection in this investigation. By using a 2D laser scanner, evenness is assessed by checking the deviation of the extracted line segments which have been mostly used to build a 2D environment map and localize a mobile robot [10], [11]. In this investigation, our novel robotic system also proposes an assessment methodology which can give the angle between the two walls accurately. To calculate this angle, a number of plane extraction methods [12]–[14] have been proposed to extract a plane from the sensor data. Finally, an inclinometer is used to assess the ground inclination. The five aforementioned defects and their corresponding automated assessment algorithms are elaborated experimentally to validate the robustness of the proposed novel assessment robot system.

The rest of this paper is organized as follows: the sensors and their related mechanisms are briefly introduced in Section II and the proposed algorithms are presented in Section III. The experimental results are given in Section IV. Finally, some conclusions are drawn from this study in Section V.

II. SENSORS AND MECHANISMS

The selected sensors for QuicaBot are shown in Fig. 2 and the related mechanisms are shown in Fig. 3. The field of view for the FLIR thermal camera is 25×18.8 degrees,

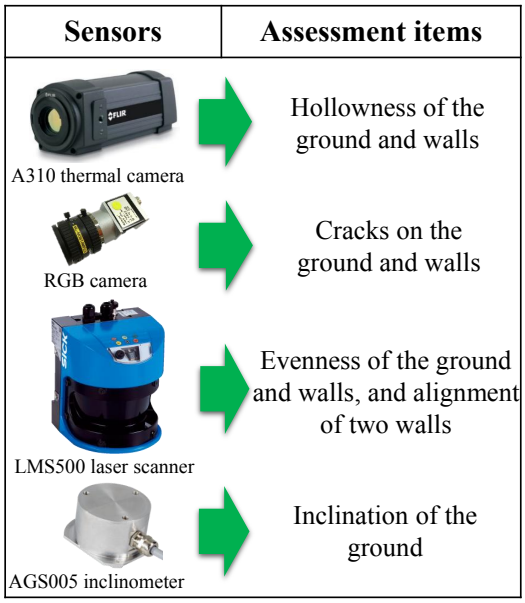

Fig. 2: Selected sensors for QuicaBot.

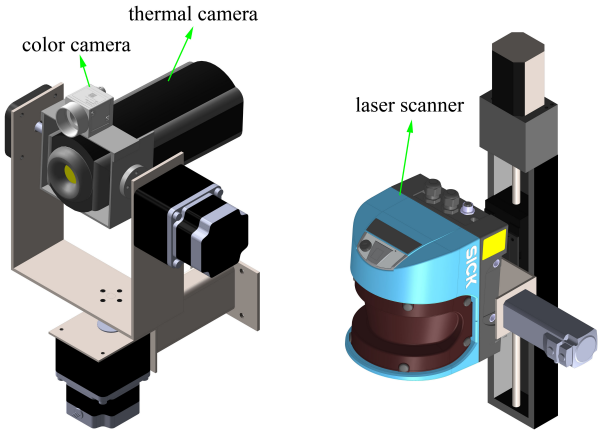

(a) Pan-tilt device. (b) Linear actuator.

Fig. 3: 3D model for the designed mechanisms.

and its working frequency is around 30Hz. This thermal camera is used to capture thermal images after heating the assessed environment for a short time by using a heater. To cover a larger capture area at a fixed location, this thermal camera is mounted on a pan-tilt device as shown in Fig. 3a. Based on the thermal images, the hollow defects can be extracted successfully. However, in the manual assessment, the inspector needs hold a metal rod and slide it inch by inch while keeping a tight contact with the assessed tiles. During this process, the hollowness is assessed by distinguishing the generated sound from the friction of the metal rod and the tiles. Even for an experienced inspector, long assessment time is needed to complete the hollowness assessment of a room unit. Moreover, the hollow shape of a tile cannot be assessed by using only the friction sound. On the other hand, in the proposed autonomous robot, it can be clearly extracted from the captured thermal image.

A low cost color camera is mounted on the top of the thermal camera to capture color images for crack assessment. Nine color images are captured in different directions by controlling the pan-tilt device while the robot is stationary. Currently, high resolution color camera are the most common method for crack assessment which has been used to detect the cracks for vessel [3] and bridge maintenance [15] successfully. When compared to the visual checking in manual assessment, automatic crack assessment can not only achieve a more accurate result in a relatively shorter time but also the length and shape of the crack can be obtained.

A SICK LMS500 laser scanner is selected to assess the evenness of the ground and walls as well as the alignment of walls. This laser scanner has a scanning range of 190 degrees with a measurement accuracy of 6 millimeters, and its maximum working frequency is 100 HZ with the measurement resolution of 1 degree. In our following set of experiments, we choose the angular resolution of 0.3333 degree with the working frequency of 50Hz. For evenness assessment, this laser scanner is mounted on a device which has a rotation range of 90 degrees. By controlling the device rotation and scanning with an interval angle of 2 degrees, 45 scans can be obtained during the assessment process which takes more samples than the five samples of the manual evenness assessment process for one wall. This laser scanner with the rotation device can also be used to construct a 3D model for the assessment environment [16].

To realize the alignment assessment, the rotation device with the laser scanner is mounted on a linear actuator as shown in Fig. 3b to obtain four 2D scans at different heights. The first two scans and the remaining two scans are respectively used to extract planes from the scanned walls for calculating the angles of adjacent walls. Traditionally, the inspectors need to keep a set square horizontally [17] while one edge is tightly contacted with one wall. The alignment of the two walls is assessed by checking the gap between the other edge of the set square and the second wall. An error may easily be introduced if the set square is not accurately held in a horizontal direction because of inspector's exhaustion or lack of experience.

Finally, a POSITAL AGS005 inclinometer is selected to assess the inclination of the ground. When compared to the spirit level of manual assessment and the strain sensors [18] for inclination estimation, this inclinometer is more appropriate to be installed on the proposed QuicaBot. This inclinometer has a measurement resolution of 0.001 degree and measurement accuracy of 0.01 degree with the measurement range of 8 degrees. In addition, the inclination angles on both x and y axes can be simultaneously obtained.

III. Assessment Algorithms

A. Hollowness assessment

Since a temperature increase on tiles with and without hollowness has significantly different characteristics, captured thermal images can be used to extract the hollow feature. In Algorithm 1, the pseudo-code of the proposed hollowness

assessment algorithm is presented. An sample image in Fig. 4 is used to illustrate the detailed procedures of the algorithm. The original image is shown in Fig. 4(a) where the maximum red value of the image is obtained due to the fact that the red color in a thermal image represents the high temperature. After blurring the image, the pixels with lower temperature than a threshold value are set as white and the contrast of the remaining pixels is reduced as in Fig. 4(b).

Algorithm 1: Proposed hollowness assessment algorithm

input : A thermal image T
output: The sum of the hollowness areas

$BlurImage \leftarrow blur(T)$;
$MaxRed \leftarrow FindMaxRGB(BlurImage)$;
for *i-th row in* $BlurImage$ **do**
  for *j-th column in* $BlurImage$ **do**
    if $BlurImage(i,j) < (MaxRed - threshold)$ **then**
      $BlurImage(i,j).SetWhite()$;
    else
      $BlurImage(i,j).ReduceContrast$;
    end
  end
end
$BlurImage.border.SetWhite()$;
$BlurImage.TopHat()$;
$GreyImage \leftarrow ColorToGrey(BlurImage)$;
$NewBlurImage \leftarrow blur(GreyImage)$;
$ContourSet \leftarrow ContourExtraction(NewBlurImage)$;
$HollowArea = 0.0$;
for *i-th contour in* $ContourSet$ **do**
  if $ContourSet[i].isclose()\&\&ContourSet[i].size() > LimNum$ **then**
    $T.plot(ContourSet[i])$;
    $HollowArea+ = ContourSet[i].area()$;
  end
end

To obtain the closed boundaries for the hollow defects, the $TopHat$ method is used, and the contours of the corresponding grey image are extracted. However, even though the image is blurred, not all the extracted contours are closed as in Fig. 4(c). As a matter of fact, the contour of a real hollow area should be closed especially filling the image borders as white. A closure state checking method is developed to check whether the extracted contour is closed or not. If the contour is closed and its length is bigger than a threshold value, the area located in the interior of this contour is considered as being the hollow defect. Eventually, the hollow areas are simultaneously summed for the features satisfying the previous hollow conditions. The original image with the plotted hollow contours is shown in Fig. 4(d).

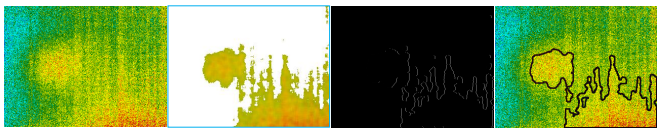

Fig. 4: (a) Original thermal image; (b) Pixels with high temperature; (c) Extracted contours; (d) Final contours plotted on the original image.

B. Crack assessment

When compared to hollowness assessment, crack assessment is more difficult because of the small size of the crack features. A detailed image processing algorithm for crack extraction is proposed in Algorithm 2, and the corresponding example for illustrating the process is shown in Fig. 5. For assessing the crack located on the tiles, the joint of the two adjacent tiles is a confusing feature because it has a similar size and color with a real crack. Therefore, it may lead an incorrect assessment result. To eliminate these types of confusions, line segments are firstly extracted from the image in Fig. 5(a) and plotted onto the original image as shown in Fig. 5(b). In the line segments extraction process, a blurred color image is firstly converted to a grey image and the edges of this image are detected. These extracted edges are taken as the input of the process of the line extraction.

Algorithm 2: Proposed crack assessment algorithm

input : A color image C
output: Boundaries of the crack defects

$BlurImage \leftarrow blur(C)$;
$GreyImage \leftarrow ColorToGrey(BlurImage)$;
$EdgeImage \leftarrow EdgeDetection(GreyImage)$;
$LineSet \leftarrow LineExtraction(EdgeImage)$;
$C.plot(LineSet)$;
$C.BlackHat()$;
$NewBlurImage \leftarrow blur(C)$;
$BinaryImage \leftarrow GreyToBinary(NewBlurImage)$;
$ContourSet \leftarrow ContourExtraction(BinaryImage)$;
for *i-th contour in* $ContourSet$ **do**
  if $ContourSet[i].size() > LimNum$ **then**
    $C.plot(ContourSet[i])$;
  end
end

Based on the image in Fig. 5(b), a $BlackHat$ method is applied to extract the crack related features. To reduce the redundant features, the output image is converted into a binary image by comparing the pixel grey value with a threshold value. The binary image with the extracted features is shown in Fig. 5(c), from which it can be seen that some small segments are incorrectly considered as cracks. A further filter method is used to neglect the small segments by checking the continuous pixel size of a candidate feature. Eventually, the contours of all the segments are extracted and the contour size is filtered with a threshold value. The

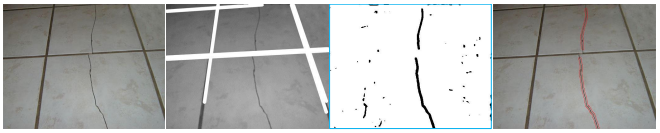

Fig. 5: (a) Original color image; (b) Blurred image with extracted line segments; (c) Binary image; (d) Extracted contours for the crack features.

final output is the original image with the filtered contours of cracks as shown in Fig. 5(d).

C. Evenness assessment

The raw sensor data coming from the 2D laser scanner should firstly divided into different groups because they may belong to different objects. In Algorithm 3, in the beginning, a group of raw data are separated into many groups in two cases. One is when measuring the distance of the two contiguous points have a big difference, the other one is that the angle of the two vectors constituted by four contiguous points is beyond a limit value. For the raw sensor data in each group, a line segment is extracted by using the least squares method. The reader is encouraged to refer to [10] for the detailed derivation of the equations for the line extraction. The average deviation of the extracted line segment is calculated and the point having the maximum deviation is selected. Each data group is further segmented as two at this selected point when the average deviation of its extracted line segment is not less than a limit value.

After extracting a line segment for each group of sensor data, the contiguous line segments need to be merged to avoid over-segmentation if these line segments belong to the same wall or ground. This merging process is realized by checking the minimum distance and angle of the two line segments. However, the short line segments extracted from less than five data points may exist in the previous segmentation. These short line segments and its neighboring line segment may lead to a large angle, but actually these two line segments may belong to the same scanned object. As a further merging process, two noncontiguous line segments satisfying the merging conditions are merged as one if at most two short line segments are located in the middle of these two line segments.

Algorithm 3: Proposed evenness assessment algorithm

input : A 2D sensor scan s
output: Line segments with eligible or ineligible flag

$GroupSet \leftarrow GroupSegment(s)$;
while *i-th group in* $\{GroupSet\}$ **do**
  $TempLine \leftarrow LineExt(GroupSet[i])$;
  if $TempLine.AveDev < LimDev$ **then**
    $LineSet.add(TempLine)$;
  else
    $(g_1, g_2) \leftarrow FurtherSegment(GroupSet[i])$;
    $GroupSet.swap(GroupSet[i], [g_1, g_2])$;
    $i = i - 1$;
  end
end
$LineSet \leftarrow LineMerge(LineSet)$;
$LineSet \leftarrow FurtherMerge(LineSet)$;
while *j-th line* l_j *in* $\{LineSet\}$ **do**
  if $l_j.MaxDev > LimMaxDev$ || $l_j.AveDev > LimAveDev$ **then**
    $l_j.flag = true$;
  else
    $l_j.flag = false$;
  end
end

When the previous segmentation and merging steps are finished, the evenness of the scanned object can be assessed by checking the average deviation or maximum deviation of the corresponding line segment. If one of these two deviations is beyond the corresponding limit value, this wall or ground is considered as uneven.

D. Alignment assessment

Alignment assessment with a laser scanner needs two 2D scans which have to be obtained in different translational heights or tilt angles. In Algorithm 4, the assumption is that the two scans are obtained and the line segments are extracted from each scan by using Algorithm 3. In the beginning, line segments of each scan with the length of longer than 0.5 meter are selected, because narrow walls are also neglected in manual inspection. Then, planes are constituted based on these two groups of line segments, and each line segment in this process is used only once. The line segments, which are used to construct planes, are disabled in the following constitution process.

For two spatial line segments, coplanarity is firstly checked by calculating the distance between one of their four endpoints and a plane constituted by other three endpoints. If this point is far from the temporarily constructed plane, these two line segments cannot constitute a plane. For a wall having an opening like a door, two line segments are extracted from raw sensor data by scanning the door part. If both scans are obtained from the door part, it is not correct that the

Algorithm 4: Proposed alignment assessment algorithm

input : Two line sets $SetOne, SetTwo$
output: All possible angles $AngleSet$

$NewSetOne \leftarrow LineSelect(SetOne)$;
$NewSetTwo \leftarrow LineSelect(SetTwo)$;
for *j-th line* l_j *in* $\{NewSetTwo\}$ **do**
  $d_j.f = false$;
end
for *i-th line* l_i *in* $\{NewSetOne\}$ **do**
  for *j-th line* l_j *in* $\{NewSetTwo\}$ **do**
    $f_1 \leftarrow IsOnSamePlane(l_i, l_j)$;
    $f_2 \leftarrow IsOverlap(l_i, l_j)$;
    $d_{ij} \leftarrow MinDis(l_i, l_j)$;
    if f_1 && f_2 && $(d_{ij} < d_*)$ && $(!d_j.f)$ **then**
      $NewPlane \leftarrow PlaneExt(l_i, l_j)$;
      $PlaneSet.add(NewPlane)$;
      $d_j.f = true$;
      break;
    end
  end
end
for *k-th plane* p_k *in* $\{PlaneSet\}$ **do**
  t = k + 1;
  for *t-th plane* p_t *in* $\{PlaneSet\}$ **do**
    $f \leftarrow IsClose(p_k, p_t)$;
    $TempAngle \leftarrow CalAngle(p_k, p_t)$;
    if f && $TempAngle < LimAngle$ **then**
      $AngleSet.add(TempAngle)$;
    end
  end
end

coplanarity condition for all combinations of these four line segments is satisfied. To avoid this case, two line segments having an overlapping segment can constitute a plane. However, for two parallel walls, extracted line segments from two parallel scans obtained in different translational heights may incorrectly construct a plane. To avoid this case, the minimum distance of the two line segments is calculated, because the two line segments far from each other may form two different walls. When all these conditions are satisfied, a new plane is extracted from the two candidate line segments.

With the extracted planes, the angles between a plane and its two neighbor planes can be calculated. In the previous plane extraction process, the four corners of each plane are obtained by projecting the four endpoints of the two line segments onto the extracted plane. To guarantee that the two planes are close, the minimum distance of these two planes are obtained by calculating the distances between the four corners of one plane and that of the other plane. Even though all possible angles of any two close planes are obtained, only the selected angles are stored, because the angle of the two walls in alignment assessments is closer to true angle.

E. Inclination assessment

Ground inclination is assessed when all the previously explained assessments are finished. This is because the inclinometer measurement needs some time to stabilize itself after the movements of robot system. The output of the inclinometer is the inclination angle in X and Y axes. To have a more accurate inclination assessment result, many groups of inclination angles in both axes are obtained and their average value is considered as the inclination angle at the fixed location. Finally, the inclination status of this location is assessed by comparing the inclination angle with a limit inclination value which is defined based on the experimental results in the following section.

IV. Experimental Results

A. Assessment of a constructed testbed

To test the designed novel robot and to validate the proposed algorithms in this paper, a testbed consisting of two walls with a size of 2m×2m each and a floor with a size of 2.2m×2.2m is constructed as shown in Fig. 6. The defects of this testbed are manually generated throughout the construction process. The angle of the two walls is manually inspected as 91.24 degrees, and the hollow defects and cracks are constructed at predefined positions. One flooring tile on the ground is also constructed as a bulgy tile. These predefined artificially generated problems on the testbed are the ground truth data for the proposed algorithms.

Before the autonomous assessment procedure starts, the two walls are heated for 30 seconds, and then the thermal images are captured while the thermal camera is $1.5m$ far away from the walls. The extracted contours for the thermal images are shown in Fig. 7 and the percentages of the hollowness areas with respect to the whole image are also described. As can be seen from the images in Fig. 7, the tiles with hollowness have higher temperature value than the perfect walls which means without any hollowness. These results are motivating in a way that a thermal camera is one of the efficient ways of assessing hollowness.

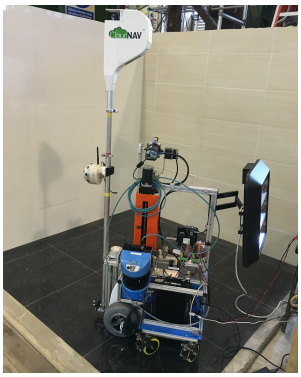

Fig. 6: Constructed testbed with QuicaBot.

When capturing the thermal images, color images are simultaneously captured. One color image with crack features is processed in Fig. 8 where the original image is shown in Fig. 8(a). It can be found that the cracks on the image are quite thin and its color is quite close to the joining color and the shadow color. By using the Algorithm 2, the extracted features are expressed as a binary image in Fig. 8(b). The contours of the filtered crack features are shown in Fig. 8(c), which still includes some incorrect features. Actually, these features can be neglected by setting a bigger threshold value. However, the real cracks may also be removed due to this operation. To include the real cracks as many as possible, the threshold value must be properly set. With the increase of experimental tests in different environments, the assessment result can be improved by using a learning and classification method based on the large number of images.

To check the performance of the laser scanner under different conditions, it is individually tested with different scanning angles by setting the inclination angle of the base

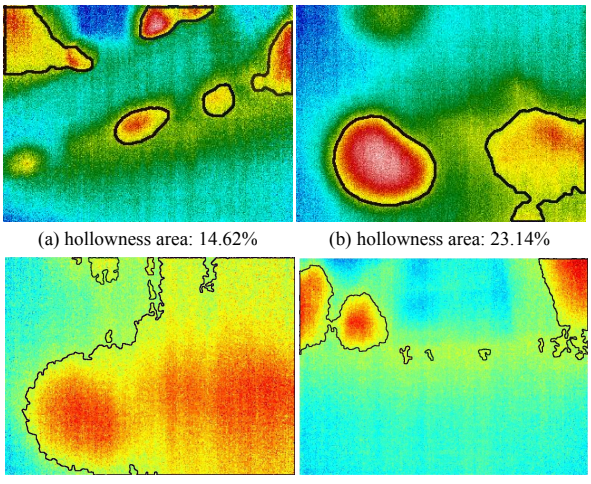

(a) hollowness area: 14.62% (b) hollowness area: 23.14%

(c) hollowness area: 72.45% (d) hollowness area: 13.25%

Fig. 7: Hollowness assessment results for the constructed testbed.

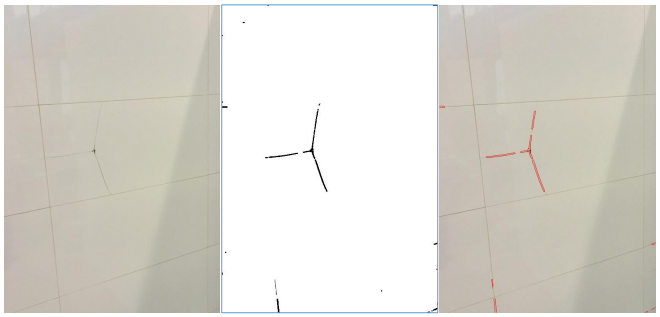

(a) (b) (c)

Fig. 8: Crack assessment for the constructed testbed: (a) Original image; (b) Binary image; (c) Color image with extracted contours.

platform. For each 2D scan, two line segments are extracted from the two scanned walls. In Fig. 9, four different cases of evenness assessment are illustrated with a schematic diagram, experiment setup, and the average deviation value for the two extracted line segments of 200 scans. By comparing the average deviation of the two line segments, it can be seen that the average deviations of wall 1 plotted with red squares are bigger than that of wall 2 plotted with blue dots for all these scans of each case. The average value of the 200 deviation values for wall 1 in all four cases are close to 4 millimeter, and that for wall 2 are smaller than 3 millimeter. Most of the deviation values of wall 2 is smaller than 3.2 millimeter defined as a limit value in the following assessment of the CONQUAS room.

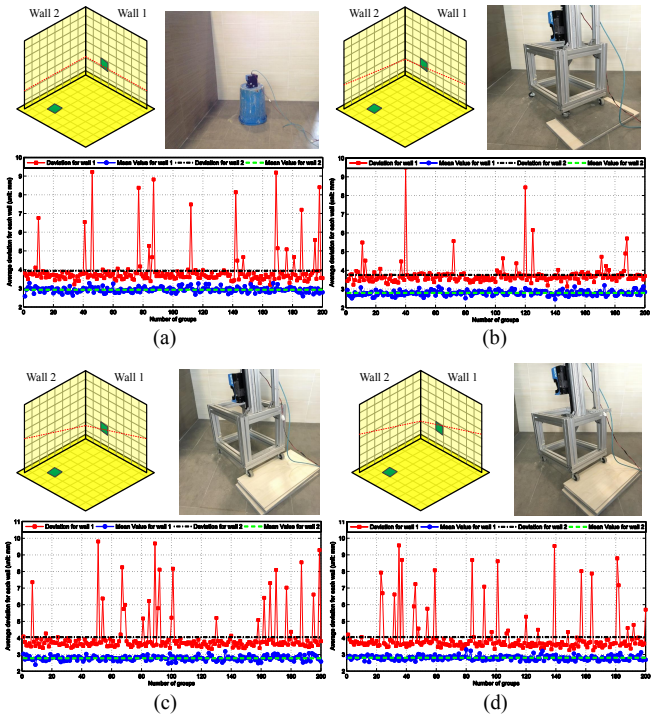

(a) (b) (c) (d)

Fig. 9: Evenness assessment: (a) Laser scanner is parallel with the floor; (b) The laser scanner is mounted on a platform with an inclination angle of 4.9 degree; (c) This inclination angle is equal to 8.13 degree. (d) Laser scanner is moved up about 15 centimeters with the same scanning direction as in (d). The schematic diagram and the figures of the experimental setup are shown in left-top and right-top respectively for each case. The average deviations of the extracted line segments for 200 scans are shown in the bottom.

The alignment of the two walls for the testbed is assessed by obtaining two 2D scans at different heights. In Fig. 10, the schematic diagram of the scanning area and an example of a constituted plane from the extracted line segments are shown. 22 groups of data are obtained, and the calculated angles of the extracted planes from these data are presented in Fig. 11. All these angle values locate from 91.3 degree to 91.6 degree, which is closer to 91.24 degree of manual inspection value. The average value of these 22 tests is about 91.43 degree plotted with a red dashed line.

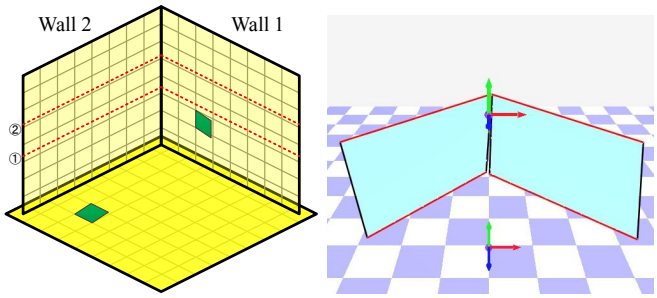

Fig. 10: Schematic diagram for evenness assessment of two walls (left), and an example of extracted plane (right).

The testbed ground is assessed by obtaining 1000 data for eight locations in Fig. 12, in which the ground on the first four locations are even. For the last four locations, the inclinometer is put on the edges of a bulgy tile. As can be seen from Fig. 13, both maximum and minimum inclination angles of the first four locations in both X and Y axes are in the limit range of $0.3 \sim 0.8$ degree. For the fifth and the eighth location, inclination angle in X is smaller than 0.3 degree and close to 4 degree respectively because the fifth location is on the middle of the tile and the eighth location is on the edge having the maximum bulgy height. The inclination values for both locations are in the limit range because this bulgy tile has accurate location in Y axis. For the sixth and seventh location, the inclination angles in both of X

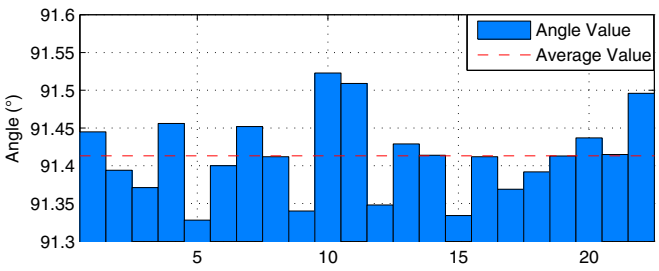

Fig. 11: Angle of the two walls of the testbed for 22 tests.

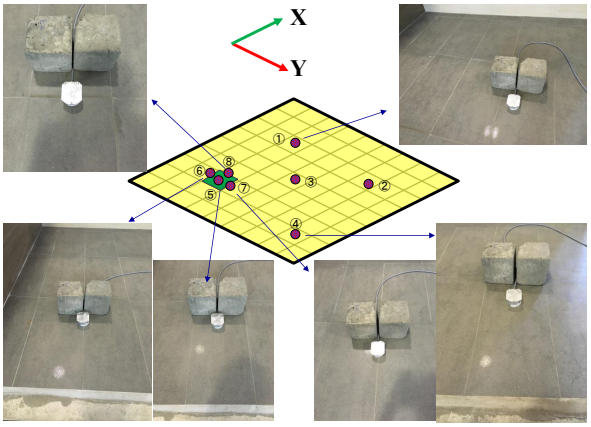

Fig. 12: Experimental setup for the inclination assessment of the testbed ground in eight different locations.

and Y axes are out of the limit range. The inclination angles in Y axis are opposite because the measurement directions of the inclinometer are opposite. The inclination angles of the fifth, sixth, seventh location in X axis are approximately the same because these three locations have the same Y axis.

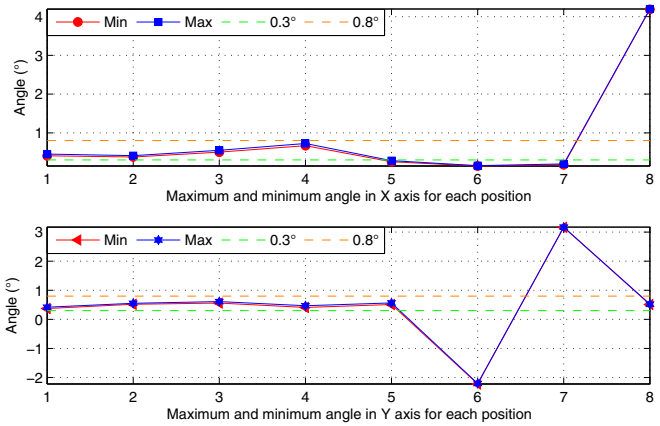

Fig. 13: Maximum and minimum inclination angle of 1000 tests for each location in X (top) and Y (bottom) direction.

V. Conclusions and Future Work

This paper proposes a novel robot for the post construction quality assessment of newly constructed building and its corresponding assessment algorithms with four sensors to automatically inspect five types of defects: hollowness, alignment, evenness, alignment and inclination. The prototype is tested in a constructed testbed to validate the robustness and accuracy of the proposed methods. All these autonomous assessments have a closer inspection accuracy with the ones in manual assessments. When compared to manual assessment, the proposed assessment system has higher effectiveness and more consistent measurement accuracy. As a future work, a user interface will be developed to display the assessment results, and the building information modeling will be integrated with the assessment results to show the defects location.

Acknowledgment

This work was supported by National Research Foundation of Singapore (NRF2015-TDIR01-03) and also the School of Mechanical and Aerospace Engineering, Nanyang Technological University, Singapore.

References

[1] R. J. Yan, C. L. Low, J. Duan, L. Liu, E. Kayacan, I. M. Chen, and R. Tiong, "Development of a novel post-construction quality assessment robot system," in *International Conference on Control, Automation, Robotics and Vision (ICARCV)*, Nov 2016, pp. 1–6.

[2] T. zaslan, K. Mohta, J. Keller, Y. Mulgaonkar, C. J. Taylor, V. Kumar, J. M. Wozencraft, and T. Hood, "Towards fully autonomous visual inspection of dark featureless dam penstocks using mavs," in *2016 IEEE/RSJ International Conference on Intelligent Robots and Systems (IROS)*, Oct 2016, pp. 4998–5005.

[3] F. Bonnin-Pascual, A. Ortiz, E. Garcia-Fidalgo, and J. P. Company, "A micro-aerial platform for vessel visual inspection based on supervised autonomy," in *2015 IEEE/RSJ International Conference on Intelligent Robots and Systems (IROS)*, Sept 2015, pp. 46–52.

[4] A. Foudazi, C. A. Edwards, M. T. Ghasr, and K. M. Donnell, "Active microwave thermography for defect detection of cfrp-strengthened cement-based materials," *IEEE Transactions on Instrumentation and Measurement*, vol. 65, no. 11, pp. 2612–2620, Nov 2016.

[5] P. Cotic, D. Kolaric, V. B. Bosiljkov, and et al, "Determination of the applicability and limits of void and delamination detection in concrete structures using infrared thermography," *NDT & E International*, vol. 74, pp. 87 – 93, 2015.

[6] W. Zhang, Z. Zhang, D. Qi, and et al, "Automatic crack detection and classification method for subway tunnel safety monitoring," *Sensors*, vol. 14, no. 10, p. 19307, 2014.

[7] H. Oliveira and P. L. Correia, "Automatic road crack detection and characterization," *IEEE Transactions on Intelligent Transportation Systems*, vol. 14, no. 1, pp. 155–168, March 2013.

[8] Y. Shi, L. Cui, Z. Qi, F. Meng, and Z. Chen, "Automatic road crack detection using random structured forests," *IEEE Transactions on Intelligent Transportation Systems*, vol. 17, no. 12, pp. 3434–3445, Dec 2016.

[9] P. Prasanna, K. J. Dana, N. Gucunski, and et al, "Automated crack detection on concrete bridges," *IEEE Transactions on Automation Science and Engineering*, vol. 13, no. 2, pp. 591–599, April 2016.

[10] R. J. Yan, J. Wu, M.-L. Shao, and et al, "Mutually converted arc-line segment-based slam with summing parameters," *Proc. IMechE, Part C: Journal of Mechanical Engineering Science*, vol. 229, no. 11, pp. 2094–2114, 2015.

[11] R. J. Yan, J. Wu, J. Y. Lee, and et al, "Representation of 3d environment map using b-spline surface with two mutually-perpendicular lrfs," *Mathematical Problem in Engineering*, vol. 2015, no. 690310, pp. 1–14, 2015.

[12] X. Qian and C. Ye, "Ncc-ransac: A fast plane extraction method for 3-d range data segmentation," *Cybernetics, IEEE Transactions on*, vol. 44, no. 12, pp. 2771–2783, Dec 2014.

[13] R. Hulik, M. Spanel, P. Smrz, and et al, "Continuous plane detection in point-cloud data based on 3d hough transform," *Journal of Visual Communication and Image Representation*, vol. 25, no. 1, pp. 86 – 97, 2014.

[14] C. Feng, Y. Taguchi, and V. Kamat, "Fast plane extraction in organized point clouds using agglomerative hierarchical clustering," in *Robotics and Automation (ICRA), IEEE International Conference on*, May 2014, pp. 6218–6225.

[15] R. S. Lim, H. M. La, Z. Shan, and et al, "Developing a crack inspection robot for bridge maintenance," in *Robotics and Automation (ICRA), IEEE International Conference on*, May 2011, pp. 6288–6293.

[16] R. J. Yan, J. Wu, J. Y. Lee, A. M. Khan, C.-S. Han, E. Kayacan, and I.-M. Chen, "A novel method for 3d reconstruction: Division and merging of overlapping b-spline surfaces," *Computer-Aided Design*, vol. 81, pp. 14 – 23, 2016.

[17] A. Ani, N. Tawil, S. Johar, and et al, "Building condition assessment for new houses: A case study in terrace houses," *Jurnal Teknologi*, vol. 70, no. 1, pp. 43–50, 2014.

[18] W. Svensson and U. Holmberg, "Estimating ground inclination using strain sensors with fourier series representation," *Journal of Robotics*, vol. 2010, no. 465618, pp. 1–8, 2010.